III International Conference on Particle-based Methods – Fundamentals and Applications
PARTICLES 2013
M. Bischoff, E. Oñate, D.R.J. Owen, E. Ramm & P. Wriggers (Eds)

FAILURE OF A GEOTEXTILE-REINFORCED EMBANKMENT USING THE MATERIAL POINT METHOD (MPM)

FURSAN M. HAMAD[1], PIETER A. VERMEER[1,2] AND CHRISTIAN MOORMANN[1]

[1] Institut für Geotechnik, Universitt Stuttgart,
Pfaffenwaldring 35, 70569 Stuttgart, Germany
fursan.hamad@igs.uni-stuttgart.de
christian.moormann@igs.uni-stuttgart.de

[2] Deltares, Stieltjesweg 2,
2600 MH Delft, the Netherlands
pieter.vermeer@deltares.nl

Key words: Material Point Method, Membrane modeling, Embankment failure

Abstract. In a wide spectrum of geotechnical applications, materials undergo large deformations and/or large displacements. On modeling these problems with a Lagrangian finite element method, the mesh can become too distorted and re-meshing is essential. In the past decades, considerable efforts have been made to adopt what is called meshfree methods to mitigate the problems related to mesh distortion. One of these methods is the Material Point Method (MPM) that represents the continuum field as Lagrangian material points (particles), which can move through the fixed background of an Eulerian mesh.

In this paper, the tensile membrane is modeled using the coupled FEM-MPM approach which adopts two-dimensional triangular elements for the membrane discretisation which is free to move through a three-dimensional mesh of non-structured tetrahedral elements. Apart from the membrane, the soil is treated with the classical procedure of MPM.

To show the potential of the method and the presented membrane scheme, a failure of an embankment with and without geotextile has been presented in this paper. The analyses of failure mechanism and the embankment stability using undrained conditions were investigated to determine the critical embankment height and the corresponding geotextile forces. For the sake of comparison, Plaxis 2D with large deformation formulation is considered as a reference solution.

1 INTRODUCTION

The reinforcement of the earth works is involving more frequently geosynthetics. Soil slopes, retaining walls, roads and embankments are some applications which often require to be stabilized mechanically be installing geotextile. To evaluate the effect of reinforcement numerically, various modeling techniques include the conventional methods derived from limit equilibrium analysis to the continuum modeling based on constitutive relationships, and micro-mechanical modeling have been performed to investigate the geosynthetic-reinforced earth structures [3].

The finite element method has the advantage over traditional analysis techniques that the displacements and stresses within the soil are coupled and depending on the constitutive model more realistic soil behavior can be represented. Early parametric studies using large deformation finite element formulations on the effects of reinforcement on stability and deformations were done by Rowe and Soderman [5] and Rowe et al. [6]. Numerical methods such as the finite element method (FEM) have the capability for modeling membranes by using a formulation that resembles to some extent the formulation of shell elements; obviously without rotational degrees of freedom. In many engineering problems large displacements and deformations occur. When these problems are modeled with a Lagrangian finite element method, the mesh can become too distorted and re-meshing is needed.

Large deformation problems can, however, be solved using so-called meshfree methods. These methods trace the history of the state variables at material points, which are not related to the element mesh. The mesh does not deform, and the problem of severe mesh distortion is overcome. One of these methods is the particle-in-cell method (PIC) which was used to model fluid dynamics in the 1960s. Sulsky and Schreyer [7] adopted the PIC for solid mechanics and gave it later the name Material Point Method (MPM). MPM has been successfully used to model several problems related to geotechnical applications, such as the discharge of granular material from a silo [10] and pile hammering [4]. York [11] developed MPM for the modeling of thin membranes, in which a 2D membrane is discretised by a collection of material points on its surface.

Later on, the membrane is represented differently in the context of MPM formulation with an application of releasing geocontainer from split barge [2]. In this approach, the surface of the membrane is discretised by a triangular mesh. The mesh connectivity is maintained during the simulation where the membrane nodes are free to move through the tetrahedral mesh. The displacement of these nodes is described by the solution of the momentum equation on the tetrahedral computational mesh, but the increment in membrane strain and stress is based on the deformation of the triangular mesh. The membrane strains and stresses are calculated at the integration point. As long as 3-noded triangular elements are adopted in this scheme, the location of the integration point could be anywhere inside the triangle and does not need to correspond to the Gaussian point. For more clarification about this membrane representation, a schematic diagram is presented

for a rectangular element with the reinforcement of a bar/membrane element embedded through the width as shown in Figure 1. In the initial configuration of this figure, an external force is applied on top. As a result, the membrane particles would follow the deformations kinematically producing in-line strain ε_ξ which in turns produces the stress σ_ξ. Accordingly, this stress is integrated along the length to get the membrane forces acting on opposite direction to the deformation. Lastly, the internal membrane force is transferred to the original mesh by weighting the location of the computational nodes relative to the membrane nodes. Further details about this scheme, the reader is recommended to see Hamad et al. [2].

2 BRIEF REVIEW OF MPM

In MPM the continuum body is discretised by Lagrangian material points as shown in Figure 2. The momentum equation is solved on the background Eulerian mesh which provides a convenient means of calculating discrete derivatives.

2.1 Spatial discretisation

The conservation of linear momentum is given by

$$\varrho\, \ddot{\boldsymbol{u}} = \nabla \cdot \boldsymbol{\sigma} + \varrho\, \boldsymbol{g} \tag{1}$$

where $\boldsymbol{\sigma}(\boldsymbol{x}, t)$ is the Cauchy stress tensor at position $\boldsymbol{x}$ and time t, $\varrho(\boldsymbol{x}, t)$ is the mass density, $\boldsymbol{g}(\boldsymbol{x}, t)$ is the gravitational acceleration vector, $\boldsymbol{u}(\boldsymbol{x}, t)$ is the displacement with the superposed dot denoting differentiation with time.
By taking the virtual displacement $\delta\boldsymbol{u}$ as test function for a domain of volume V surrounded by boundary S, the weak form of the momentum equation can be written as

$$\begin{aligned}\int_V \delta\boldsymbol{u}^T \varrho\, \ddot{\boldsymbol{u}}\, dV = &\int_V \delta\boldsymbol{\varepsilon}^T \boldsymbol{\sigma}\, dV + \int_V \delta\boldsymbol{u}^T \varrho\, \boldsymbol{g}\, dV \\ &+ \int_{S_t} \delta\boldsymbol{u}^T \boldsymbol{t}\, dS\end{aligned} \tag{2}$$

where $\boldsymbol{t} = \boldsymbol{\sigma} \cdot \boldsymbol{n}$ is the prescribed traction on boundary S_t, $\boldsymbol{n}$ is the outward unit normal and the script T denotes the transpose. Similar to the standard finite element method, the value of a variable inside the element can be based on the nodal values and the nodal shape functions. For example, the displacement vector can be written as

$$\boldsymbol{u}(\boldsymbol{x}, t) = \boldsymbol{N}\boldsymbol{a} \qquad \text{and} \qquad \delta\boldsymbol{u} = \boldsymbol{N}\delta\boldsymbol{a} \tag{3}$$

where $\boldsymbol{N}$ is a matrix containing global shape functions over the whole computational grid and $\boldsymbol{a}$ is the nodal displacement. Using these definitions and discretising the momentum

Equation 2, it takes the form [10],

$$\boldsymbol{M}\,\ddot{\boldsymbol{a}} = \boldsymbol{F}^{ext} - \boldsymbol{F}^{int} \tag{4}$$

where $\boldsymbol{M}$ is the consistent mass matrix, $\ddot{\boldsymbol{a}}$ the nodal acceleration vector, $\boldsymbol{F^{ext}}$ and $\boldsymbol{F^{int}}$ are the external and internal nodal force vectors respectively. The mass matrix is given by

$$\boldsymbol{M} = \sum_{p=1}^{n_p} m_p\,\boldsymbol{N}^T(\boldsymbol{x}_p)\,\boldsymbol{N}(\boldsymbol{x}_p) \tag{5}$$

where n_p is the number of material points and m_p is the mass of material point p at location $\boldsymbol{x}_p$. However, in practice, the lumped mass matrix is preferred over the consistent mass matrix. This simplifies the computations at the expense of introducing a slight amount of numerical dissipation [1]. The lumped mass matrix $\boldsymbol{M}_l$ is the diagonal matrix. The structure of the lumped mass matrix is as follows

$$\boldsymbol{M}_l = \begin{bmatrix} m_1 & 0 & \cdots & 0 \\ 0 & m_2 & \cdots & 0 \\ \vdots & \vdots & \ddots & \vdots \\ 0 & 0 & \cdots & m_n \end{bmatrix} \tag{6}$$

where n is the total number of degrees of freedom which could increase or decrease within the calculation as particles move between elements. However, each component of the diagonal term (m_i) in Equation 6 being the corresponding row sum of the consistent matrix is performed as

$$m_i \approx \sum_{p=1}^{n_p} m_p\; N_i(\boldsymbol{x}_p) \tag{7}$$

Referring to Equation 4, the internal force vector yields

$$\boldsymbol{F}^{int} = \sum_{p=1}^{n_p} V_p\;\; \boldsymbol{B}^T(\boldsymbol{x}_p)\;\; \boldsymbol{\sigma}_p \tag{8}$$

where the quotient of the material point mass and density is the volume of the material point, $V_p = m_p/\varrho_p$ and $\boldsymbol{B}$ is the strain-displacement matrix, as also used in standard finite element method [10], $\boldsymbol{\sigma}_p$ is a vector containing the stress components at the material point p. The external nodal force vector is given by

$$\boldsymbol{F}^{ext} = \sum_{p=1}^{n_p} m_p\;\; \boldsymbol{N}^T(\boldsymbol{x}_p)\;\; \boldsymbol{g} + \int_{S_t} \boldsymbol{N}^T\;\boldsymbol{t}\;dS \tag{9}$$

2.2 Time integration

So far the momentum Equation 4 is defined and needs to be solved for discrete time intervals. With the mass matrix being a diagonal matrix, solving the system of equations becomes trivial, i.e.,

$$\ddot{\boldsymbol{a}}^t = [\boldsymbol{M}_l^t]^{-1} \boldsymbol{F}^t \tag{10}$$

in which, Euler-forward time integration scheme is applied to update the nodal velocity from nodal acceleration. However, a slightly different algorithm is applied to obtain nodal velocity by updating particles velocity first in the form [8]

$$\dot{\boldsymbol{a}}_p^{t+\Delta t} = \dot{\boldsymbol{a}}_p^t + \sum_{i=1}^{n} \Delta t \, N_i \left(\boldsymbol{x}_p\right) \, \ddot{\boldsymbol{a}}_i^t \tag{11}$$

where Δt is the current time increment, $\dot{\boldsymbol{a}}_p^t$ and $\dot{\boldsymbol{a}}_p^{t+\Delta t}$ are the velocities of particle p at time t and $t + \Delta t$, respectively. As next the velocity field is mapped from the particles to the grid considering that the momentum should be conserved, i.e.,

$$\boldsymbol{M}_l^t \, \dot{\boldsymbol{a}}^{t+\Delta t} = \sum_{i=1}^{n_p} m_p \, \boldsymbol{N}^T \left(\boldsymbol{x}_p\right) \, \dot{\boldsymbol{a}}_p^{t+\Delta t} \tag{12}$$

where $\dot{\boldsymbol{a}}^{t+\Delta t}$ is the updated nodal velocity which is used to get the incremental displacements $\boldsymbol{a}^{t+\Delta t}$ as

$$\boldsymbol{a}^{t+\Delta t} = \Delta t \, \dot{\boldsymbol{a}}^{t+\Delta t} \tag{13}$$

The positions of the particles are subsequently updated from

$$\boldsymbol{x}_p^{t+\Delta t} = \boldsymbol{x}_p^t + \boldsymbol{N}_p \, \Delta \boldsymbol{a}^{t+\Delta t} \tag{14}$$

where $\boldsymbol{x}_p^t$ and $\boldsymbol{x}_p^{t+\Delta t}$ are the particle positions at time t and $(t + \Delta t)$ respectively.
For the present MPM solution procedure, a slightly different algorithm has been adopted for updating the particles velocity following Sulsky et al. [8].
By solving the equation of motion for the nodes, the elements deform and the material points in the interior of the element move in proportion to the motion of the nodes, based on the nodal basis functions. The position of the material points is updated using a single-valued continuous velocity field and, hence the interpenetration of material is precluded. This automatic feature of the algorithm allows simulations of no-slip contact between different bodies without the need for special interface tracking and contact algorithms.
After getting the grid node velocities, the strain increment $\Delta \boldsymbol{\varepsilon}_p$ of the material point p at time $(t + \Delta t)$ is calculated from,

$$\Delta \boldsymbol{\varepsilon}_p^{t+\Delta t} = \Delta t \; \boldsymbol{B} \left(\boldsymbol{x}_p\right) \; \dot{\boldsymbol{a}}_e^{t+\Delta t} \tag{15}$$

where $\dot{\boldsymbol{a}}_e^{t+\Delta t}$ is the vector of nodal velocities of the element e which the material point belongs to. Based on the calculated strain increment, the stress increment $\Delta\boldsymbol{\sigma}_p^{t+\Delta t}$ at each material point is updated by applying the appropriate constitutive model. The constitutive models are applied at material points and this allows easy evaluation and tracking of history-dependent variables. It also allows computations with more than one material, since each material point retains its material properties throughout the computation, for example in the modeling of soil/membrane interaction.
As the mass of the material point m_p is kept constant during the calculation, the density of the material is implicitly updated by updating the volume of the material point through

$$V_p^{t+\Delta t} = V_p^t \left(1 + \Delta\varepsilon_{v,p}^{t+\Delta t}\right) \tag{16}$$

where $\Delta\varepsilon_{v,p}$ is the incremental volumetric strain of the material point p computed from the incremental strain components ($\Delta\varepsilon_v = \Delta\varepsilon_x + \Delta\varepsilon_y + \Delta\varepsilon_z$) in (x, y, z) coordinates.
At the end of time $(t + \Delta t)$ all the material point variables are updated and a new cycle is begun using the information carried by the material points to initialise nodal values on the grid. Note that at this stage, a new grid can be defined since all the state variables are carried by the material points. In practice however, the most efficient way is to keep the original grid.

3 STABILITY OF A GEOTEXTILE-REINFORCED EMBANKMENT

The test embankments of Almere in the Netherlands which were constructed in 1979 are back calculated by many references [5, 9]. In which, two embankments were built on a soft clay deposit to measure the effect of geotextile reinforcement upon stability as shown in Figure 3. Therefore, one of them is reinforced with geotextile whilst the other served as a non-reinforced reference. After constructing the retaining bank on the subsoil, each embankment was loaded by hydraulic sand filling. At failure, the reinforced one reordered a sand height of 3 $[m]$ while the non-reinforced failed at a height of 1.75 $[m]$ [9].

3.1 Assumptions and material modeling

For the numerical model requirements, boundaries need to be established at certain length and each medium should follow certain constitutive model. The strong peaty sand layer underneath will serve as a fixed bottom for the numerical model while the side boundaries are assumed rigid in the horizontal directions. The soil is simplified as an elastoplastic material with a Mohr-Coulomb failure criterion. The geotextile is treated as linear elastic with an axial stiffness of 1900 $[kN/m]$ and negligible flexural rigidity, in addition to, it assumed to be rough enough that failure would happen inside the soil.

The construction procedure was reported such that the ditch was excavated in the clay layer while at the same time the retaining bank was made with the excavated clay.

Table 1: Properties of the soils

parameter	symbol	clay	sand
saturated weight	γ_{sat} $[kN/m^3]$	20	20
stiffness	E $[kN/m^2]$	1043	4000
Poisson's ratio	ν $[-]$	0.49	0.35
cohesion	c $[kN/m^2]$	10	1
friction angle	ϕ $[^\circ]$	0	32
dilatancy angle	ψ $[^\circ]$	0	2

As next, the hydraulic fill with fully saturated sand was achieved. In this analysis, the embankment is constructed sufficiently quick that consolidation of the subsoil is negligible. For the filling loose sand, the shear modulus should be proportional to the pressure level which is averaged with a constant value in this study. The mechanical properties of the embankment and the filling sand are listed in Table 1 [9].

3.2 Reference solution (Plaxis)

Although the embankment test was achieved in field, no detailed information available about failure. However, the only available information is the height of the sand layer at failure. Therefore, the finite element software (Plaxis 2D) with the formulation of large deformation has been considered as a reference solution for this study. In which, a 6-node triangular element for the plane-strain problem was adopted.

Following the classical procedure of phase construction, the embankment is built by having the subsoil layer with ($K_0 = 1$) followed by second phase of removing the ditch and constructing the retaining bank. Finally, the loading phase is performed by gradually increasing the unit weight of the 3 $[m]$ height of sand. The horizontal displacement of the toe point is recorded as a control point. Solution obtained with Plaxis 2D will be shown in the context of this paper as a reference for the MPM solution. Figure 4 shows the mesh discretisation related to Plaxis model with the corresponding boundary conditions.

3.3 MPM solution

In MPM, the embankment problem is modeled using 4-node tetrahedral elements with 10 particles initially placed in each element. Here, the K_0 procedure is not considered, whereas, the gravity load of the retaining bank is applied in 10 load steps. As the MPM procedure followed dynamic formulation, some local damping has been added to obtain the quasi-static solution by reducing the kinetic energy equally over all degrees of freedom. After constructing the retaining bank, the gravity weight of the sand particles increased

in step wise manner with a step value of 2 $[kN/m^3]$. As low order elements are adopted in the MPM, volumetric locking is expected especially for the clay with high value of Poisson's ratio. Therefore, a strain smoothening technique is applied to enhance the performance of the tetrahedral elements [4].

For the non-reinforced embankment, total displacement at the end of sand filling is shown in Figure 4 for the MPM as compared with Plaxis. Even though the load-displacement curve of the toe shows some scattering of the MPM solution around the FEM curve, the total displacement contour shows great match between the two solutions with successful prediction for the maximum displacements of 1.2 $[m]$ under the ditch.

Similar to the non-reinforced embankment, the reinforced one predicts good agreement between MPM and FEM as demonstrated in Figure 5. In this figure, the explicit nature of the MPM scheme is clearly illustrated in the deviation from the implicit FEM solution. However, the vertical stress distribution of both solutions show stress oscillation at the failed integration points as seen in Figure 6. Nevertheless, the failure mechanism of both schemes match quite well after using the strain enhancement technique. For the developed forces in the geotextile, the MPM underpredict these forces, Figure 7, which can be attributed by referring to Figure 5 which predicts less deformation in MPM.

4 CONCLUSIONS AND OUTLOOK

In the paper, the material point method MPM has been shown its ability to model a geomechanical problem of reinforced embankment with geotextile where the dynamic MPM formulation with local damping is used to solve the quasi-static problem. The plane-strain problem is modeled successfully in three-dimensional MPM using tetrahedral elements. The use of low order element with MPM is mitigated by using the strain smoothening technique. Deformations and stresses produced by MPM show a good quality as compared with the finite element software Plaxis.

Furthermore, the coupled FEM-MPM membrane modeling is validated for large deformation problem where rough contact with soil is assumed. This approach shows very good agreement with the updated Lagrangian FEM. However, the underestimation of the stresses along the MPM geotextile can be corresponded to the MPM soil deformation which shows less values as compared with FEM.

Although rough contact is assumed between the soil and the geotextile in this study, frictional contact can be modeled as well [2]. More advanced contact modeling by involving adhesion is necessary in the future. Moreover, studying the effect of consolidation by adopting two-phase analysis is an essential issue for investigating the real dynamic behavior.

References

[1] D. Burgess, D. Sulsky, and JU Brackbill. Mass matrix formulation of the flip particle-in-cell method. *Journal of Computational Physics*, 103(1):1–15, 1992.

[2] F.M. Hamad, P.A. Vermeer, and C. Moormann. Development of a coupled FEM-MPM approach to model a 3D membrane with an application of releasing geocontainer from barge. *Installation Effects in Geotechnical Engineering*, pages 176–183, 2012.

[3] J. Huang, A. Bhandari, and X. Yang. Numerical modeling of geosynthetic-reinforced earth structures and geosynthetic-soil interactions. *Geotechnical Engineering*, 42(1): 43, 2011.

[4] I.J. Jassim, F.M. Hamad, and P.A. Vermeer. Dynamic material point method with applications in geomechanics. In *2nd International Symposium on Computational Geomechanics (COMGEO II)*, Cavtat-Dubrovnik, Croatia, 27-29 April 2011.

[5] R. K. Rowe and K. L. Soderman. Comparison of predicted and observed behaviour of two test embankments. *Geotextiles and Geomembranes*, 1(2):143–160, 1984.

[6] R. K. Rowe, M. D. MacLean, and K. L. Soderman. Analysis of a geotextile-reinforced embankment constructed on peat. *Canadian Geotechnical Journal*, 21(3):563–576, 1984.

[7] D. Sulsky and H.L. Schreyer. A particle method with large rotations applied to the penetration of history-dependent materials. *Advances in Numerical Simulation Techniques for Penetration and Perforationof Solids, ASME, AMD*, AMD-Vol 171: 95–102, 1993.

[8] D. Sulsky, S.J. Zhou, and H.L. Schreyer. Application of a particle-in-cell method to solid mechanics. *Computer Physics Communications*, 87(1):236–252, 1995.

[9] H. van Langen. *Numerical Analysis of Soil-Structure Interaction*. PhD thesis, Delft University of Technology, Delft, The Netherlands, 1991.

[10] Z. Wieckowski, S.K. Youn, and J.H. Yeon. A particle-in-cell solution to the silo discharging problem. *International journal for numerical methods in engineering*, 45 (9):1203–1226, 1999.

[11] A. R. York. *The development of modifications to the material point method for the simulation of thin membranes, compressible fluids, and their interactions*. PhD thesis, The University of New Mexico, 1997.

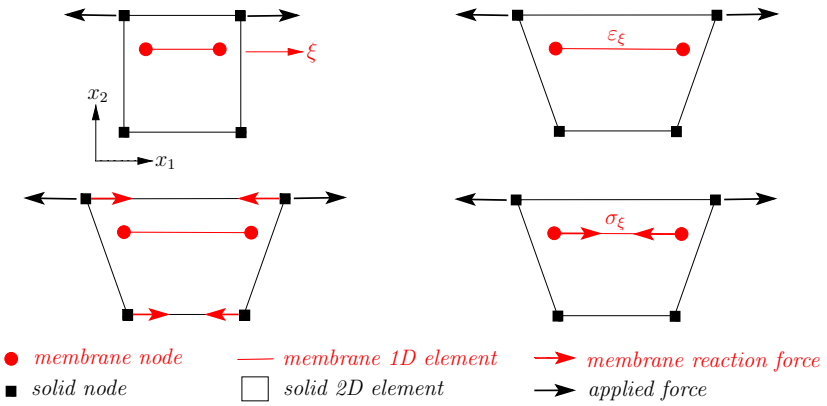

Figure 1: Schematic diagram of the coupled FEM-MPM approach. Clockwise from top left: initial configuration, deformed configuration, stress integration and forces mapping

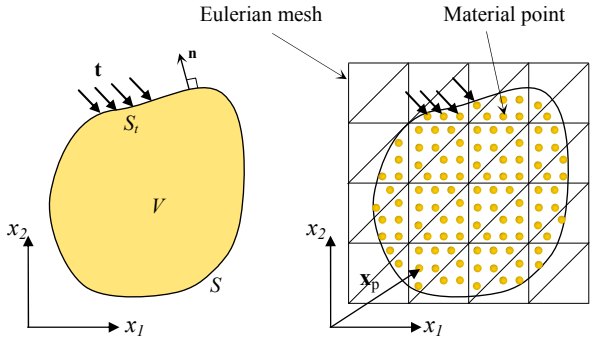

Figure 2: Continuum body (left) represented by MPM (right)

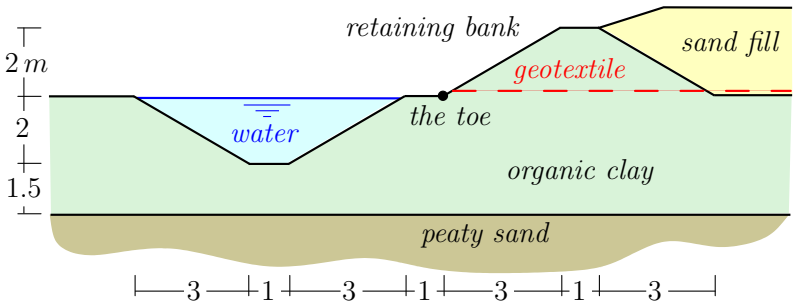

Figure 3: Almere test embankment reinforced with geotextile

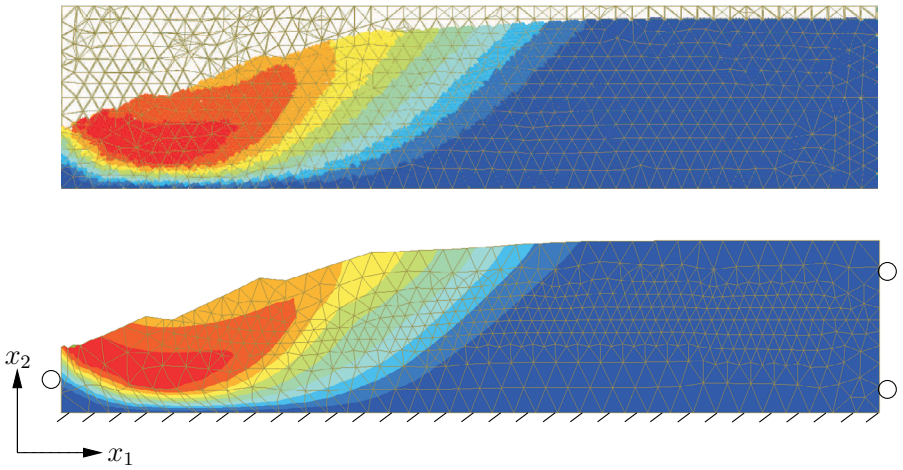

Figure 4: Total displacements of the non-reinforced embankment; blue color is zero displacement and red is 1.2 m: (bottom) Plaxis 2D and (top) MPM

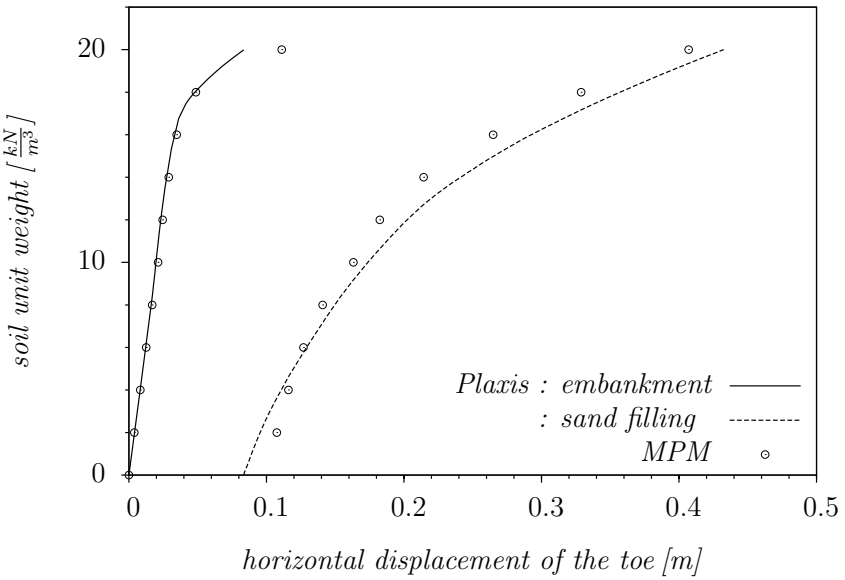

Figure 5: Horizontal displacement of the toe for the reinforced embankment

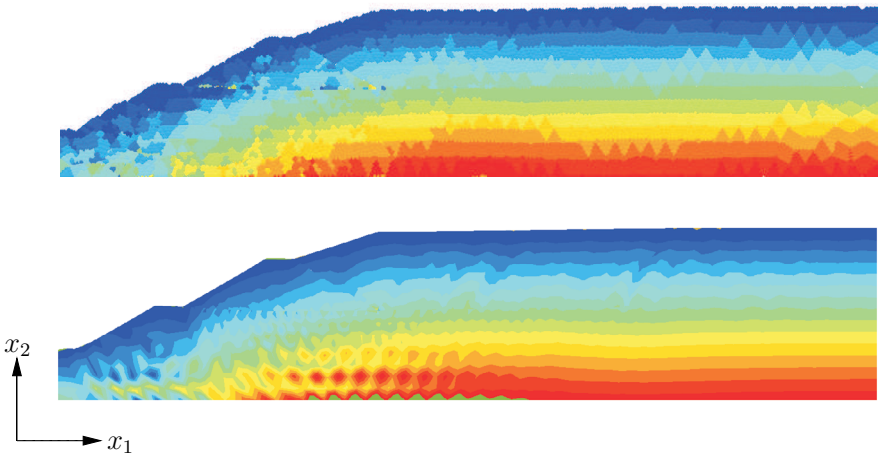

Figure 6: Total vertical stress for the reinforced embankment; blue color is zero stress and red is $-130\,kN/m^2$: (bottom) Plaxis 2D and (top) MPM

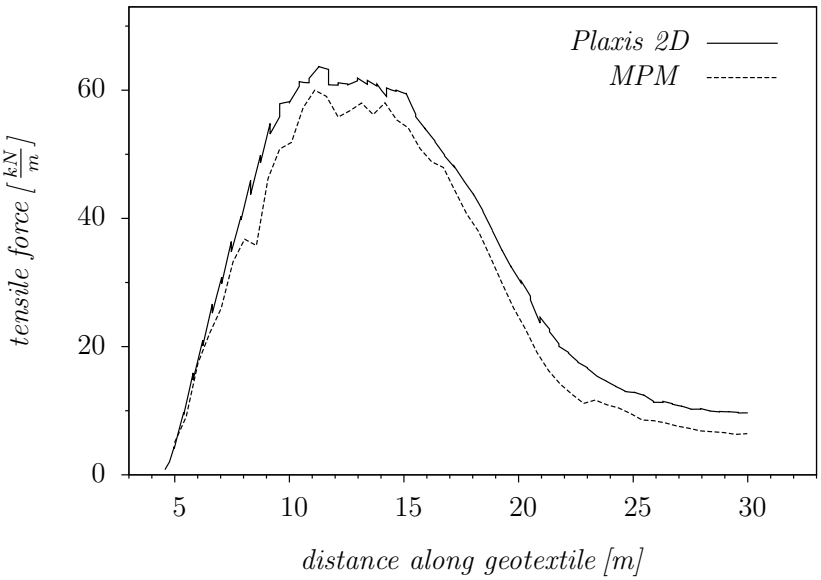

Figure 7: Comparison of the tensile forces along the geotextile